Check for updates

ChemPubSoc Europe

DOI: 10.1002/batt.201900029

BATTERIES & SUPERCAPS
Articles

Computational Insights into Mg-Cl Complex Electrolytes for Rechargeable Magnesium Batteries

Jared B. Moss,[a] Liping Zhang,[a] Kevin V. Nielson,[a] Yujing Bi,[a] Chao Wu,*[b] Steve Scheiner,*[a] and T. Leo Liu*[a]

DFT calculations were conducted to provide unprecedented thermodynamic insights on tetrahydrofuran (THF) solvation, isomerization, and complexation of possible Mg–Cl coordination species for popular Mg–Cl electrolytes for magnesium batteries. Computational results using the M06-2x functional with the 6-31 + G(d) basis set indicate that trigonal bipyramidal *e,e-cis-tbp*-$MgCl_2(THF)_3$ dichloride species and octahedral $[MgCl(THF)_5]^+$ monochloride species are the dominant mononuclear species. These two can combine to form the dinuclear species $[(\mu\text{-}Cl)_3Mg_2(THF)_6]^+$ with a free energy −6.30 kcal/mol, which is calculated to be the dominant Mg–Cl species in solution. Two mono-cation species, $[(\mu\text{-}Cl)_3Mg_2(THF)_6]^+$ and $[MgCl(THF)_5]^+$, have comparable LUMO energies, thus both of them can act as active species for Mg deposition. However, the significant dominance of the dinuclear species in the electrolyte indicates that it is the primary species involved in reversible Mg deposition.

1. Introduction

To meet increasing energy density demands, advanced batteries are greatly desired for powering portable devices, electric vehicles (EVs), and grid-scale energy storage that are pivotal to our daily life and the economic development of the modern society.[1–3] Thus far, rechargeable Li ion batteries have gained tremendous success in portable electronic devices and power tools, and have been recently employed as a power source for electrical vehicles (EVs) which reduces the use of fossil fuels and emission of CO_2.[1–3] However, technological limitations of Li-ion batteries including low energy density, high cost, and safety issues have called on the development of the next generation of battery technologies.[1–3] Beyond Li-ion batteries, pure metal battery systems such as Li batteries and Na batteries are highly attractive for electrochemical energy storage because of their high energy densities,[1–3] but have not been implemented due to a number of technical issues associated with these highly reactive pure metals including severe dendrite formation and irreversible depletion of electrolyte solvents.[4,5]

Recently, rechargeable Mg batteries have been advocated as promising battery system alternatives to Li- or Na-based batteries because of a number of technological advantages.[6–11] Mg is earth abundant and low cost (ca. 24 times cheaper than Li). As an anode material, Mg is safe to use due to its milder reactivity compared to Li and Na. Mg has a high volumetric capacity (3832 Ah/L vs 2062 Ah/L for Li and 1165 Ah/L for Na) due to the two-electron redox chemistry of the $Mg^{2+/0}$ redox couple. Furthermore, Mg possesses a sufficiently negative reduction potential (−2.37 vs SHE) amenable for assembling high voltage and high energy density batteries with suitable cathode materials. There are increasing research efforts in developing advanced Mg electrolytes, cathode materials, and anode materials for Mg and Mg ion batteries.[6–11]

Berand et al.[12] in 1971 and Gregory et al.[13] in 1990 reported the use of Al or B Lewis acid additives to enhance electrochemical performance of organomagnesium compounds (MgR_2 or RMgCl where R can be alkyl or aryl groups), which laid down a substantial foundation for the later development of Mg electrolytes. Since then, numerous Mg electrolytes for rechargeable Mg batteries have been developed using a general synthetic strategy by combining a Mg precursor as Lewis base and a Al or B based Lewis acid in ethereal solvents (THF, DME, and other glyme solvents) by a number of groups including us,[14–41] which has achieved reversible Mg cycling with overpotential less than 300 mV and anodic stability greater than 3 V vs Mg. When chloride (Cl^-) is present in the Mg or Lewis acid precursor, the resulting Mg electrolytes can be classified as Mg–Cl electrolytes in which the electrochemical active species are characteristic of the Mg–Cl bonding structure feature. Particularly, a common $[(\mu\text{-}Cl)_3Mg_2(THF)_6]^+$ dinuclear species crystal structure (Scheme 1) has been frequently observed in electrochemically active Mg–Cl electrolytes in THF.[14,15,21,42–47] In addition, it is worth noting that there have been ongoing efforts in developing Cl-free Mg^{2+} electrolytes to avoid the corrosion of chloride with low-cost current collectors such as stainless steel. Simple Mg salts including $Mg(TFSI)_2$ and $Mg(PF_6)_2$ were confirmed as not working for reversible Mg

[a] J. B. Moss, L. Zhang, K. V. Nielson, Dr. Y. Bi, S. Scheiner, T. L. Liu
Department of Chemistry and Biochemistry
Utah State University, Logan, USA, 84318
E-mail: leo.liu@usu.edu
steve.scheiner@usu.edu
[b] Prof. Dr. C. Wu
Frontier Institute of Science and Technology
Xi'an Jiaotong University
Xian, China, 710054
E-mail: chaowu@xjtu.edu.cn

Supporting information for this article is available on the WWW under https://doi.org/10.1002/batt.201900029

© 2019 Wiley-VCH Verlag GmbH & Co. KGaA, Weinheim

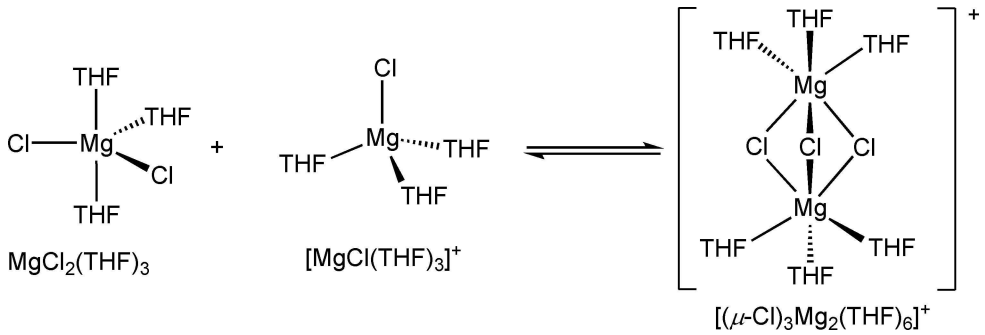

Scheme 1. Proposed equilibrium of the dinuclear species $[(\mu\text{-Cl})_3Mg_2(THF)_6]^+$ with $MgCl_2(THF)_3$ and $[MgCl(THF)_3]^+$.

deposition due to the instability of anions with Mg metal.[46,48] Magnesium carborane,[49–51] Magnesium hexafluoroisopropylaluminate,[52] Magnesium hexafluoroisopropylborate,[53–55] and Magnesium perfluorinated pinacolatoborate[56] salts were reported as rare examples of Cl-free non-corrosive electrolytes for reversible Mg deposition.

We have made contributions in developing Mg–Cl electrolytes with improved anodic stability and electrophile compatibility by avoiding the use of reactive and nucleophilic Mg sources such as Grignard reagents or dialkyl magnesium.[16–19] Specifically, we developed a facile approach (termed mono-Cl abstraction, Scheme 1) using $MgCl_2$ and an Al Lewis acid ($AlCl_3$, $AlEtCl_2$ and $AlPh_3$) to produce high-performance Mg–Cl electrolytes.[16–19] In comparison to the reported formulations using organometallic magnesium precursors and Al or B based Lewis acids, the $MgCl_2$/Al Lewis acid electrolytes are much more synthetically feasible in terms of the cost of the starting materials, purification requirements, and demonstrated improved electrochemical and chemical properties.[10,16–19] It is worth noting that the all-inorganic $MgCl_2/AlCl_3$ electrolytes in ethereal solvents represent the simplest Mg electrolyte formula to date and has attracted extensive experimental[24,25,28,32,39] and theoretical[57] studies. More recently, by using Mg powder as a scavenger to address contaminating issues of water and other deleterious impurities,[18,58] we developed a series of ternary $Mg/MgCl_2/AlCl_3$ electrolytes in THF, DME, and diglyme (termed MMAC electrolytes), which demonstrated outstanding electrochemical performance with Coulombic efficiency up to 100%, overpotential less than 220 mV, and anodic stability up to 3.8 V vs Mg.[19]

For the popular Mg–Cl electrolytes, $[(\mu\text{-Cl})_3Mg_2(THF)_6]^+$ dinuclear species was proposed to be in equilibrium with $MgCl_2(THF)_3$ and $[MgCl(THF)_3]^+$ (Scheme 1).[7,10,17] It remains in debate whether the dinuclear species or the mononuclear $[MgCl(THF)_5]^+$ is the dominant species responsible for electrochemical Mg cycling.[10,14,17,57,59] However, there are very limited experimental studies to examine the chemical constituents of the Mg–Cl electrolytes in the solution phase. One major challenge is the dynamic behaviors of labile THF coordination with Mg^{2+} cation and possible structural rearrangements, and thus, it is difficult to apply a suitable spectroscopic tool to pinpoint individual molecular species in the electrolyte solution. Arthur et al. applied X-ray absorption spectroscopy (XAS) studies to show that the dominant cation species in Mg–Cl electrolytes including $EtMgCl/Et_2AlCl$ and $[(\mu\text{-Cl})_3Mg_2(THF)_6][AlCl_4]_2$ is the dinuclear species.[60] We have reported the use of a soft mass spectrometry technique to identify a $[MgCl(THF)_3]^+$ species present in the $[(\mu\text{-Cl})_3Mg_2(THF)_6]^+$ electrolyte, providing the first experimental indication for the mononuclear $[MgCl]^+$ species in the electrolyte solution.[17] Sa et al. reported the detection of the dinuclear species species using mass spectrometry in the $MgCl_2/Mg(TFSI)_2$ (2:1 ratio) electrolyte in THF.[36] Andrew et al. suggested the existence of the $[(\mu\text{-Cl})_3Mg_2(THF)_6]^+$ dinuclear species in the $MgCl_2/AlCl_3$ solution through X-ray pair distribution function (PDF) analysis.[61] The above experimental results are inspiring, but not definitive, to elucidate the solution nature of the $[(\mu\text{-Cl})_3Mg_2(THF)_6]^+$ electrolyte. In short, we still lack a full picture of the solution chemistry of the $[(\mu\text{-Cl})_3Mg_2(THF)_6]^+$ electrolyte. Herein, we report an investigation of the $[(\mu\text{-Cl})_3Mg_2(THF)_6]^+$ electrolyte using a DFT computational approach. In addition to further understanding experimental results, DFT calculations can provide insights into the most prevalent Mg species in solution and shed light on the active species participating in reversible Mg deposition.

In this study, we adopted the M06-2x functional with 6–31 + G(d) basis set and the SMD universal solvation model with an ultrafine integration grid to elucidate the solution chemistry of the Mg electrolytes. Our DFT study provides comprehensive results to: 1) elucidate the chemical nature of possible Mg–Cl mononuclear, dinuclear, and trinuclear species in the Mg–Cl electrolytes in THF; 2) offer a systematic evaluation of structural isomers and solvation chemistry of Mg–Cl species in THF, which has never been done before; and 3) elucidate the thermodynamics for the formation of the well-known $[(\mu\text{-Cl})_3Mg_2(THF)_6]^+$ dinuclear species, giving valuable insights to previous experimental works done on this system.[21–25] Consistent with experimental results,[17,60,61] but contrary to previous DFT results,[57,62] our comprehensive DFT calculations on THF solvation, isomerization, and complexation of possible Mg–Cl species reveal that the $[(\mu\text{-Cl})_3Mg_2(THF)_6]^+$ dimer is the most dominant Mg–Cl species in solution. Hence, the presented computational results indicate the $[(\mu\text{-Cl})_3Mg_2(THF)_6]^+$ dinuclear species is the primary active species involved in Mg deposition and stripping.

© 2019 Wiley-VCH Verlag GmbH & Co. KGaA, Weinheim

25666223, 2019, 9, Downloaded from https://chemistry-europe.onlinelibrary.wiley.com/doi/10.1002/batt.201900029 by University of Ulsan, Wiley Online Library on [11/11/2025]. See the Terms and Conditions (https://onlinelibrary.wiley.com/terms-and-conditions) on Wiley Online Library for rules of use; OA articles are governed by the applicable Creative Commons License

2. Results

2.1. Computational Methods

Calculations of the Mg and Al Lewis acid systems were performed using the Gaussian 09 package[20]. The molecules and complexes were modeled as isolated molecules at 298.15 K. The systems were calculated using the M06-2X[63] functional, Minnesota'06 2x global hybrid functional with 54% Hartree-Fock exchange, with a basis set of 6–31 + G(d).[64,65] The M06-2x functional has been shown to be a more suitable choice for calculations involving thermodynamic data in main group elements and significantly outperforms B3LYP when involved in coordination chemistry of organometallics.[66–68] Compared to the B3LYP functional, the M06-2x method has demonstrated a much better correlation to experimental data involving main group elements, especially when thermodynamic data is considered.[66,67,69] To model the implicit solvent, the SMD universal solvation model[70] was used, which is based on the quantum mechanical charge density of a solute molecule interacting with a continuum description of the solvent. All molecular geometries were relaxed in the implicit THF solvent using SMD[70] at the M06-2x/6-31 + G(d) level of theory with an ultrafine integration grid to increase the accuracy of all calculations. True minima were confirmed for all optimized geometries by verifying the absence of imaginary frequencies. All optimized geometries are given in the Supporting Information.

2.2. Solvation Chemistry of $MgCl_2$

For the formation of the $[(\mu\text{-Cl})_3Mg_2(THF)_6][AlCl_4]$ electrolyte, the $MgCl_2$ reactant is the Mg precursor. Thus, the solvation chemistry of $MgCl_2$ in THF was first modeled by adding THF molecules for coordination one at a time in THF solvent until fully coordinated with $MgCl_2$, as seen in the Scheme 2 where the free energies of reaction are given in kcal/mol. Solvation of $MgCl_2$ with one THF to form $MgCl_2(THF)$ gives a large free energy of reaction of −12.61 kcal/mol. Adding another THF to form $MgCl_2(THF)_2$ leads to a tetrahedral geometry at a favorable free energy of −12.11 kcal/mol.

Further solvation of the tetrahedral mononuclear species can form $MgCl_2(THF)_3$ species, of which six different minima were found. To distinguish between the square pyramidal and trigonal bipyramidal geometries, the geometry index (τ) was calculated based on the two greatest bonding angles within each found minima as described in Addison's work.[71] The geometry index (τ) is calculated as (β-α)/60, where β is the largest angle consisting of the metal center and two ligands found in a penta-coordinate metal complex and α is the angle consisting of the metal center and other two different ligands, equal or second to β. τ = 0 indicates a square pyramidal geometry while τ = 1 indicates a trigonal bipyramidal geometry. Values below 0.5 indicate the geometry is closer to square pyramidal and above 0.5 is trigonal bipyramidal. In Scheme 2, all $MgCl_2(THF)_3$ isomers are labelled with α and β angles. Acronyms including "a", "e", "cis", "tran", "sq" and "tbp" are used and explained in Scheme 2 to name the different isomers of the $MgCl_2(THF)_3$ species. The most favorable isomer is the *e,e-cis-tbp*-$MgCl_2(THF)_3$ (I) species where both chloride ligands are in the equatorial position forming at a free energy of −3.08 kcal/mol. Two other isomers (II) and (III) of *e,e-cis-tbp*-$MgCl_2(THF)_3$ with slightly different τ values were also optimized with less favorable free energy (see Scheme 2). However, the *a, a-trans-tbp*-$MgCl_2(THF)_3$ isomer could not be optimized with the M06-2x functional since this conformation freely decayed to the *e,e-cis-tbp*-$MgCl_2(THF)_3$ (I) trigonal bipyramidal geometry. Therefore, it was optimized at the B3LYP level with all other parameters kept the same as the other calculations followed by a single point calculation with the M06-2x theory. This isomer was calculated to be the least unfavorable by 7.15 kcal/mol. This is consistent with the other observed minima where the free energies were less favorable when geometry index (τ) was close to 1 (fully trigonal bipyramidal) or 0 (fully square pyramidal). The structure becomes most relaxed when the geometries are between the index of 0.5 to 0.7 giving the least amount of angle strain and steric hinderance from the bulky THF ligands.

From *e,e-cis-tbp*-$MgCl_2(THF)_3$ (I), a fully coordinated species is obtained having two *cis*/*trans* isomers with an octahedral structure. Both show an unfavorable solvation processes at 5.28 kcal/mol for the *trans* and 4.70 kcal/mol for the *cis* being the more stable of the two. Hence, the DFT results suggests *e,e-cis-tbp*-$MgCl_2(THF)_3$ (I) is the most populated solvated $MgCl_2$ species which will be the conformation considered in further calculations. These results are qualitatively consistent with previously DFT results reported by Burk et al.[72] using B3LYP functional with a 6–31 + G(d) basis set, but different from what was reported by others (see discussions below).[57,62]

2.3. Solvation Chemistry of $[MgCl]^+$

As previously proposed, *e,e-cis-tbp*-$MgCl_2(THF)_3$ (I) needs to undergo mono-Cl abstraction with a Lewis acid such as $AlCl_3$ to form THF solvated $[MgCl]^+$ species in order to form the dinuclear species, $[(\mu\text{-Cl})_3Mg_2(THF)_6]^+$.[10,16] Therefore, Mg monochloride species were considered to characterize relevant reactions. The solvation of $[MgCl]^+$ in THF is shown in Scheme 3 as a step-wise process. Adding a THF to $[MgCl]^+$ to form the linear $[MgCl(THF)]^+$ is highly spontaneous by −13.87 kcal/mol. Addition of another THF to form the trigonal planar $[MgCl(THF)_2]^+$ species experiences a similar thermodynamic favorability of −14.89 kcal/mol, and one more THF forms the tetrahedral $[MgCl(THF)_3]^+$ at −16.74 kcal/mol. Further solvation of the tetrahedral mononuclear species formed five isomers with the chloride either in the *axial* position or the *equatorial* position. Addison's geometry index (τ) was also used to distinguish between square pyramidal and trigonal bipyramidal isomers.[71] The most favorable isomer is *a-sp*-$[MgCl(THF)_4]^+$ with a free energy of −7.86 kcal/mol where the Mg atom is left with a vacant site. Two *e-sp*-$[MgCl(THF)_4]^+$ isomers with slightly different τ values were optimized (See Scheme 3). The *a-tbp*-

© 2019 Wiley-VCH Verlag GmbH & Co. KGaA, Weinheim

25666223, 2019, 9, Downloaded from https://chemistry-europe.onlinelibrary.wiley.com/doi/10.1002/batt.201900029 by University of Ulsan, Wiley Online Library on [11/11/2025]. See the Terms and Conditions (https://onlinelibrary.wiley.com/terms-and-conditions) on Wiley Online Library for rules of use; OA articles are governed by the applicable Creative Commons License

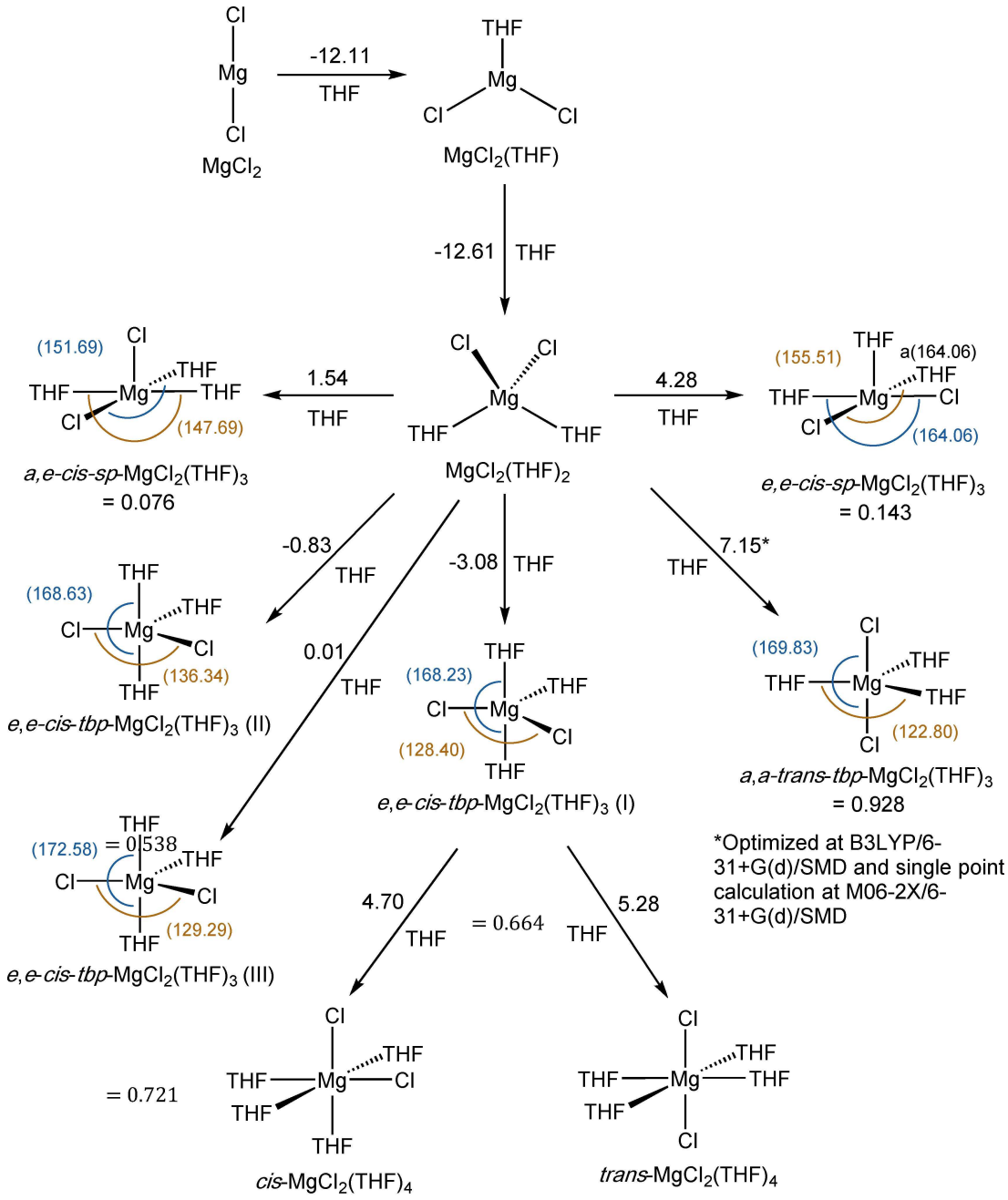

Notes about abbreviations:
"*a*" indicates a Cl^- ligand occupying an axial position;
"*e*" indicates a Cl^- ligand occupying an equatorial position;
"*cis*" indicates two Cl^- ligands lie on the same side in a given plane;
"*trans*" indicates two Cl^- ligands lie on the opposite side in a given plane;
"*sp*" indicates a molecular geometry of square bipyramidal;
"*tbp*" indicates a molecular geometry of trigonal bipyramidal.

Scheme 2. Synthesis pathway and optimisation of isomers.

$[MgCl(THF)_4]^+$ isomer could not be optimized with the M06-2x functional since this isomer freely decayed to the *a-sp*-$[MgCl(THF)_4]^+$ square pyramidal geometry. Therefore, it was optimized at the B3LYP level with all other parameters kept the same as the other calculations followed by a single point calculation with the M06-2x theory. This isomer was calculated to be the least favorable as its formation energy (−0.77 kcal/mol) is less negative than those of other *sp* isomers. Moving

© 2019 Wiley-VCH Verlag GmbH & Co. KGaA, Weinheim

25666223, 2019, 9, Downloaded from https://chemistry-europe.onlinelibrary.wiley.com/doi/10.1002/batt.201900029 by University of Ulsan, Wiley Online Library on [11/11/2025]. See the Terms and Conditions (https://onlinelibrary.wiley.com/terms-and-conditions) on Wiley Online Library for rules of use; OA articles are governed by the applicable Creative Commons License

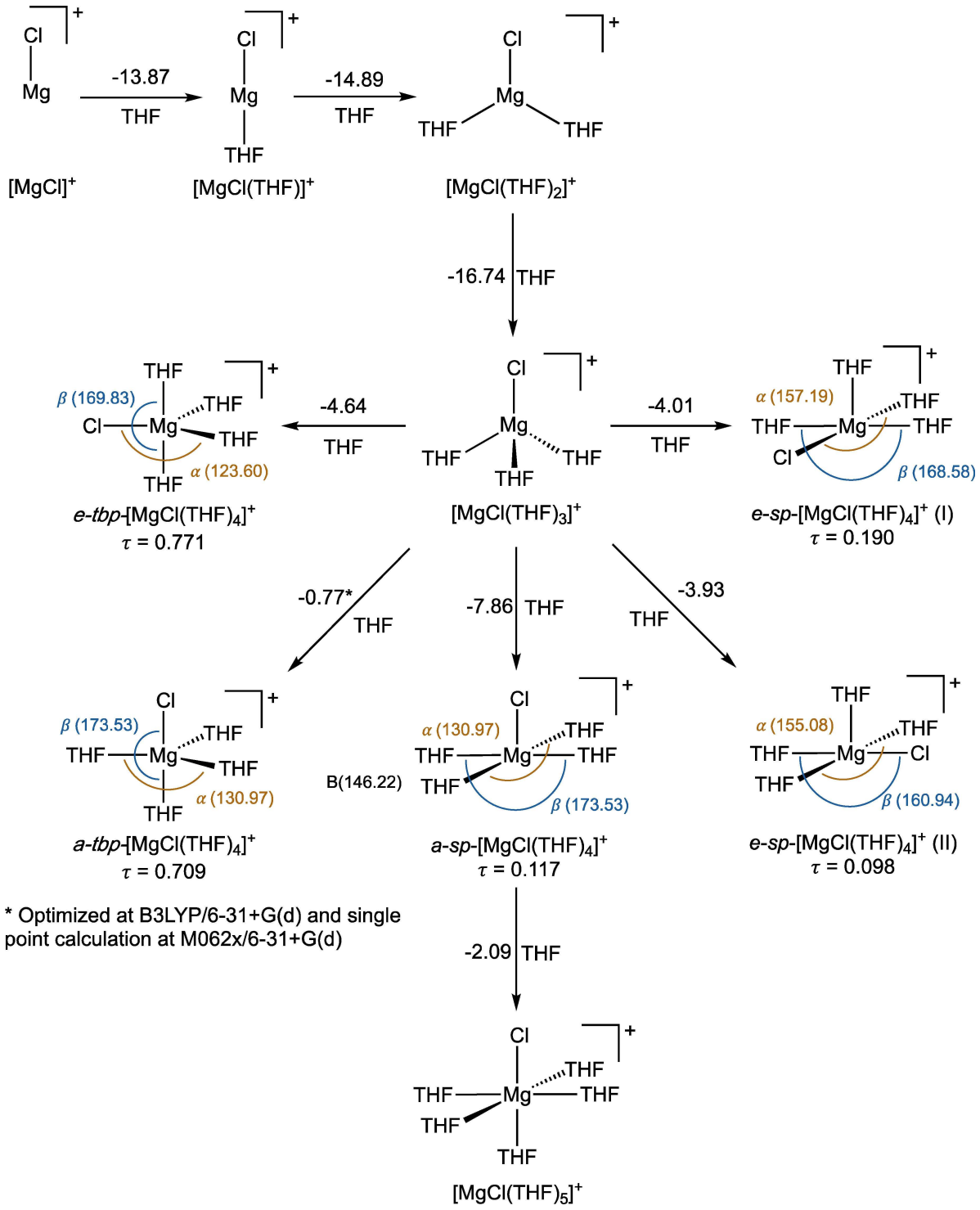

Scheme 3. Step-wise solvation of $[MgCl]^+$ in THF.

from the *axial* square pyramidal geometry of *a-sp*-$[MgCl(THF)_4]^+$ to form the octahedral six-coordinate species $[MgCl(THF)_5]^+$ is favorable by −2.09 kcal/mol. Hence, the octahedral six-coordinate species is the most populated Mg monochloride species in THF solution. According to these DFT calculations results, removal of one chloride from *e,e-cis-tbp*-$MgCl_2(THF)_3$ (I) yields $[MgCl(THF)_3]^+$ as the product which will experience further solvation to form the more stable $[MgCl(THF)_5]^+$ species.[10,16]

© 2019 Wiley-VCH Verlag GmbH & Co. KGaA, Weinheim

25666223, 2019, 9, Downloaded from https://chemistry-europe.onlinelibrary.wiley.com/doi/10.1002/batt.201900029 by University of Ulsan, Wiley Online Library on [11/11/2025]. See the Terms and Conditions (https://onlinelibrary.wiley.com/terms-and-conditions) on Wiley Online Library for rules of use; OA articles are governed by the applicable Creative Commons License

2.4. Formation of the Dinuclear and Trinuclear Species

We then considered the thermodynamics of the formation of the $[(\mu\text{-Cl})_3Mg_2(THF)_6]^+$ dinuclear species from the Mg monochloride and dichloride species to determine if it exists as such in solution. Stepwise THF solvation of the $[(\mu\text{-Cl})_3Mg_2]^+$ fragment confirms that each Mg center prefers an octahedral geometry with three THF terminal ligands and three bridging chloride ligands (Scheme 4). The formation of the $[(\mu\text{-Cl})_3Mg_2(THF)_6]^+$ is statistically expected by combination of the two most populated $[MgCl]^+$ and $MgCl_2$ species in solution, as seen in Scheme 4. Forming the dinuclear species from 1:1 ratio of *e,e-cis-tbp*-$MgCl_2(THF)_3$ (I) and $[MgCl(THF)_5]^+$ is substantially spontaneous by −6.30 kcal/mol. The relaxed geometries of the discussed solvated mononuclear and dinuclear Mg–Cl species is shown in Figure 1.

It is possible that two $[MgCl]^+$ monomers undergo self-dimerization to form a $[(\mu\text{-Cl})_2Mg_2(THF)_6]^{2+}$ dimer. By varying the number of THF coordination as well as finding a stable dimer with two bridging chlorides, the $[(\mu\text{-Cl})_2Mg_2]^{2+}$ species was most stable with each Mg having a coordination number of six, *i.e.*, $[(\mu\text{-Cl})_2Mg_2(THF)_8]^{2+}$ (Scheme S1). However, the free energy of reaction for the formation of $[(\mu\text{-Cl})_2Mg_2(THF)_8]^{2+}$ from two $[MgCl(THF)_5]^+$ monomers is unfavorable by 10.90 kcal/mol (Scheme 5).

The trinuclear species, $[(\mu\text{-Cl})_5Mg_3(THF)_6]^+$, was proposed as a possible equilibrium species for the $MgCl_2/AlCl_3$ electrolyte by Gewirth et al.[25] The formation of this trinuclear species through interaction between $[(\mu\text{-Cl})_3Mg_2(THF)_6]^+$ and an additional *e,e-cis-tbp*-$MgCl_2(THF)_3$ (I) is an unfavorable process by 4.18 kcal/mol, as seen in Scheme 6. Therefore, it can be assumed that the $[(\mu\text{-Cl})_3Mg_2(THF)_6]^+$ dinuclear species is the dominant species in the THF electrolyte solution.

3. Discussion

Calculated structural parameters of $[(\mu\text{-Cl})_3Mg_2(THF)_6]^+$, *trans*-$MgCl_2(THF)_4$, and $[MgCl(THF)_5]^+$ species are in good agreement with the experimental values of the corresponding structures determined by X-ray single-crystal diffraction (see details in Table S1), indicating the reliability of the selected calculation method. According to above DFT results, solvated $MgCl_2$ primarily exists as the *e,e-cis-tbp*-$MgCl_2(THF)_3$ (I) five-coordinated species while the $[MgCl]^+$ species mainly adopts an octahedral $[MgCl(THF)_5]^+$ geometry. In our previous study, identification of $[MgCl(THF)_3]^+$ by SPIN-MS confirms the mono-

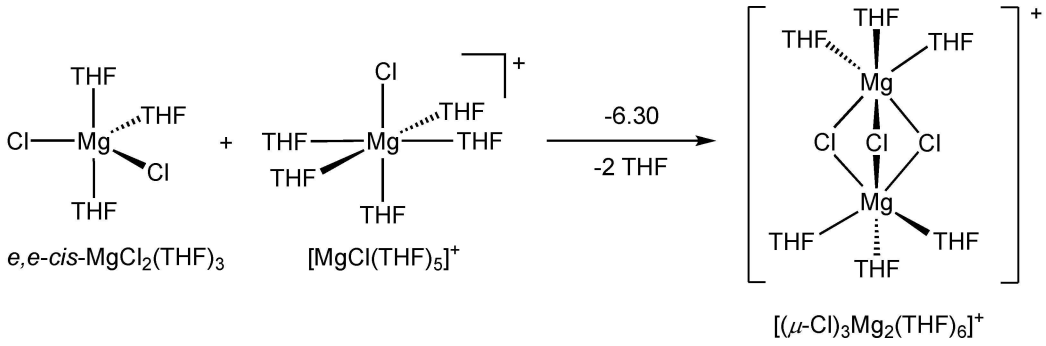

Scheme 4. Fvorable formation of $[(\mu\text{-Cl})_3Mg_2(THF)_6]^+$ from e,e,-*cis*-$MgCl_2(THF)_3$ and $[MgCl(THF)_5]^+$ and monomers.

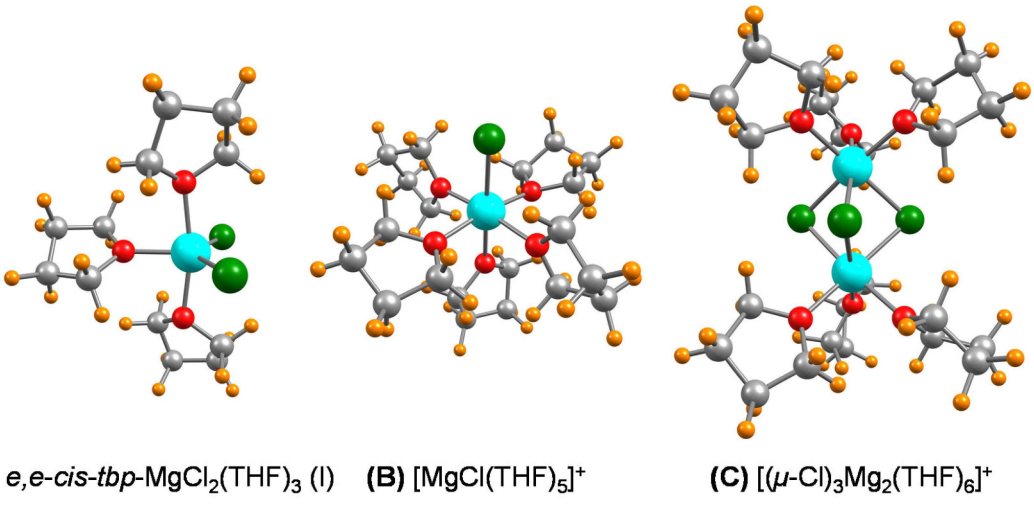

Figure 1. Optimized structures of (A) *e,e-cis-tbp*-$MgCl_2(THF)_3$ (I), (B) $[MgCl(THF)_5]^+$, and (C) $[(\mu\text{-Cl})_3Mg_2(THF)_6]^+$.

© 2019 Wiley-VCH Verlag GmbH & Co. KGaA, Weinheim

25666223, 2019, 9, Downloaded from https://chemistry-europe.onlinelibrary.wiley.com/doi/10.1002/batt.201900029 by University of Ulsan, Wiley Online Library on [11/11/2025]. See the Terms and Conditions (https://onlinelibrary.wiley.com/terms-and-conditions) on Wiley Online Library for rules of use; OA articles are governed by the applicable Creative Commons License

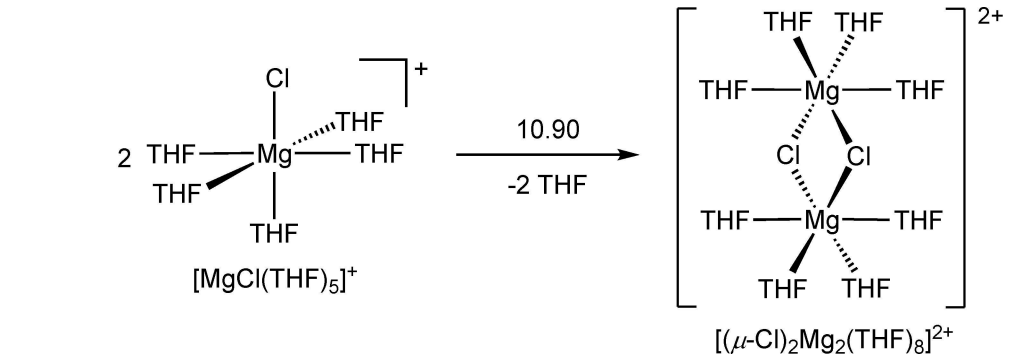

Scheme 5. Unfavorable formation of $[(\mu\text{-Cl})_2Mg_2(THF)_8]^{2+}$ from two $[MgCl(THF)_5]^+$ monomers.

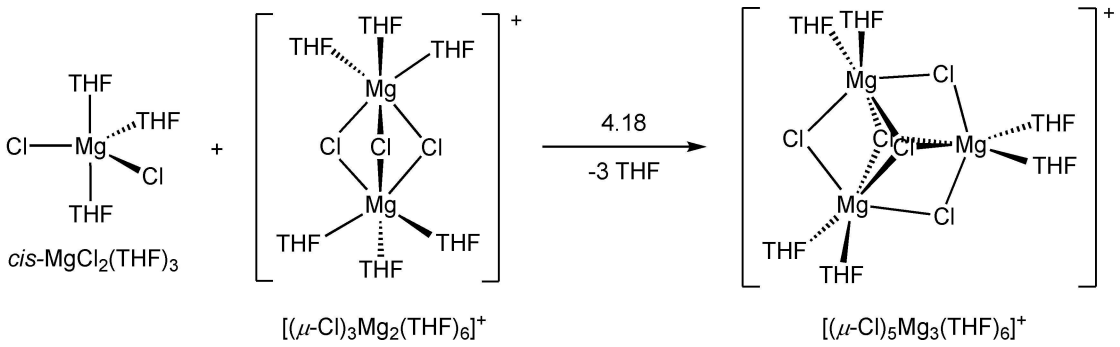

Scheme 6. Formation of trinuclear $[(\mu\text{-Cl})_5Mg_3(THF)_6]^+$ species through interaction between $[(\mu\text{-Cl})_3Mg_2(THF)_6]^+$ and an additional *e,e-cis-tbp*-$MgCl_2(THF)_3$ (I).

Cl abstraction reaction taking place between *e,e-cis-tbp*-$MgCl_2(THF)_3$ (I) and a Lewis acid.[17,19] As $[MgCl(THF)_5]^+$ is 10.7 kcal/mol more stable than $[MgCl(THF)_3]^+$, the latter species detected by SPIN-MS is believed to be formed from the former during gasification in the SPIN-MS test due to labile Mg-THF interaction (see Figure S1). From the DFT results, further removal of a THF ligand from $[MgCl(THF)_3]^+$ is much more difficult, requiring 16.74 kcal/mol to break the Mg-THF bond.

Formation of the $[(\mu\text{-Cl})_3Mg_2(THF)_6]^+$ dinuclear species from *e,e-cis-tbp*-$MgCl_2(THF)_3$ (I) and $[MgCl(THF)_5]^+$ is thermodynamically favorable by −6.30 kcal/mol in solution, and thus, the dinuclear species represents the major species in solution, which accounts for why the dinuclear species has been commonly observed in single crystal XRD studies and is also consistent with other spectroscopic studies.[60,61] The trinuclear species, $[(\mu\text{-Cl})_5Mg_3(THF)_6]^+$, is less favorable than the $[(\mu\text{-Cl})_3Mg_2(THF)_6]^+$ dinuclear species with a free energy of reaction of 4.18 kcal/mol (Scheme 6). However, when excess $MgCl_2$ species is present, the ratio of the trinuclear species can be increased, which accounts for the ^{25}Mg NMR chemical shift when the exogenous chloride was added to the $[(\mu\text{-Cl})_5Mg_3(THF)_6]AlPh_3Cl$ electrolyte.[17] It is also worth noting that if organomagnesium compounds are used as Mg ion precursors with a Lewis acid at different ratios, then the equilibrium $[(\mu\text{-Cl})_5Mg_3(THF)_6]^+$ with other Mg^{2+} species can be more complex.[16] The present DFT work only considers the equilibrium of $[(\mu\text{-Cl})_5Mg_3(THF)_6]^+$ with Mg–Cl mononuclear species.

By comparing the LUMO energy of both species, we found that $[MgCl(THF)_5]^+$ has a lower LUMO than $[(\mu\text{-Cl})_3Mg_2(THF)_6]^+$ by 0.51 kcal/mol, which indicates $[MgCl(THF)_5]^+$ is easier to reduce (Figure 2). When subject to a one-electron reduction, the redox potential difference between two mono-cations is only 22 mV. Even the $[MgCl(THF)_3]^+$ mono-cation, the direct equilibrium species of $[(\mu\text{-Cl})_3Mg_2(THF)_6]^+$, is only favored by 1.83 kcal/mol or 79 mV over the dinuclear species. In terms of thermodynamics, both $[(\mu\text{-Cl})_3Mg_2(THF)_6]^+$ and $[MgCl(THF)_5]^+$ mono-cations are almost equivalent for Mg deposition in terms of thermodynamics, which supports our previous hypothesis that both mono-cations could be active species for Mg deposition.[17] However, as $[(\mu\text{-Cl})_3Mg_2(THF)_6]^+$ is significantly more dominant than $[MgCl(THF)_5]^+$, it is expected to be primarily involved in Mg deposition.

Ceder[57] and Wan[62] reported first attempts to provide computational insights on the solvation structures and thermodynamics of $[(\mu\text{-Cl})_3Mg_2(THF)_6]^+$ and Mg–Cl mononuclear species. Their calculations promoted us to consider structural isomerization of various Mg–Cl species. It is commonly known that structural isomers can have distinct free energies, and thus, present other viable avenues by which the dinuclear species could be formed in THF solution. In addition, compared to the B3LYP and PBE functional methods used in previous studies,[57,62] the M06-2x method has demonstrated a much better correlation to experimental data involving main group elements, especially when thermodynamic data are considered.[66,67,69] Finally, previous studies[57,62] only optimized

© 2019 Wiley-VCH Verlag GmbH & Co. KGaA, Weinheim

25666223, 2019, 9, Downloaded from https://chemistry-europe.onlinelibrary.wiley.com/doi/10.1002/batt.201900029 by University of Ulsan, Wiley Online Library on [11/11/2025]. See the Terms and Conditions (https://onlinelibrary.wiley.com/terms-and-conditions) on Wiley Online Library for rules of use; OA articles are governed by the applicable Creative Commons License

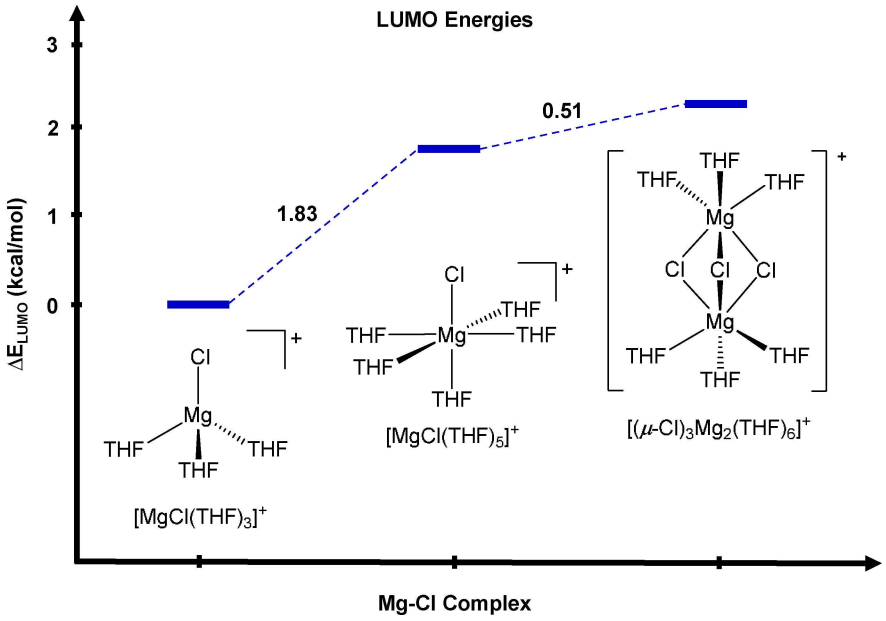

Figure 2. Relative LUMO energies of selected Mg–Cl complexes.

structures in a vacuum without considering an appropriate solvation model which is well-known to have significant effects on geometry optimization further the accuracy of free energy.

4. Conclusions

The present DFT computational studies provided a detailed picture on coordination chemistry of Mg–Cl complexes in the $[(\mu\text{-}Cl)_3Mg_2(THF)_6]^+$ electrolyte solution. The formation of the $[(\mu\text{-}Cl)_3Mg_2(THF)_6]^+$ dinuclear species from *e,e-cis-tbp*-$MgCl_2(THF)_3$ (I) and $[MgCl(THF)_5]^+$ is calculated to be thermodynamically favorable. Complementary to the previous experimental studies, the calculation results suggest that the dinuclear species is the dominant species primarily involved in Mg deposition. These computational studies provide a comprehensive and in-depth understanding of the $[(\mu\text{-}Cl)_3Mg_2(THF)_6]^+$ electrolytes and can inspire future mechanistic studies of Mg deposition for the next generation Mg electrolytes.

Author Contributions

L.L., C.W. and S.S. conceived the presented idea. L.L. and J.M. wrote the manuscript. J.M. performed the computations and analyzed data. L.Z. helped on verifying calculations. All authors discussed the results within the final manuscript and made contributions to revise the manuscript.

Acknowledgements

We thank Utah State University for providing faculty startup funds to the PI (T. Leo Liu) and the Utah Science Technology and Research initiative (USTAR) UTAG award for supporting this study. C. W. acknowledges National Natural Science Foundation of China (No. 21477096) for supporting his work. Computational resources from the Division of Research Computing in the Office of Research and Graduate Studies at Utah State University are gratefully acknowledged.

Conflict of Interest

The authors declare no conflict of interest.

Keywords: Batteries · Energy storage · Mg batteries · Mg electrolytes · Mg deposition

[1] M. Armand, J. M. Tarascon, *Nature* **2008**, *451*, 652–657.
[2] J. B. Goodenough, K.-S. Park, *J. Am. Chem. Soc.* **2013**, *135*, 1167–1176.
[3] B. Dunn, H. Kamath, J.-M. Tarascon, *Science* **2011**, *334*, 928–935.
[4] W. Xu, J. Wang, F. Ding, X. Chen, E. Nasybulin, Y. Zhang, J.-G. Zhang, *Energy Environ. Sci.* **2014**, *7*, 513–537.
[5] B. Liu, J.-G. Zhang, W. Xu, *Joule* **2018**, *2*, 833–845.
[6] K. Xu, *Chem. Rev.* **2014**, *114*, 11503–11618.
[7] H. D. Yoo, I. Shterenberg, Y. Gofer, G. Gershinsky, N. Pour, D. Aurbach, *Energy Environ. Sci.* **2013**, *6*, 2265–2279.
[8] J. Muldoon, C. B. Bucur, T. Gregory, *Chem. Rev.* **2014**, *114*, 11683–11720.
[9] P. Canepa, G. Sai Gautam, D. C. Hannah, R. Malik, M. Liu, K. G. Gallagher, K. A. Persson, G. Ceder, *Chem. Rev.* **2017**, *117*, 4287–4341.
[10] S. He, K. V. Nielson, J. Luo, T. L. Liu, *Energy Storage Mater.* **2017**, *8*, 184–188.
[11] N. N. Rajput, T. J. Seguin, B. M. Wood, X. Qu, K. A. Persson, *Top. Curr. Chem.* **2018**, *376*, 19.
[12] A. Brenner, *J. Electrochem. Soc.* **1971**, *118*, 99–100.
[13] T. D. Gregory, R. J. Hoffman, R. C. Winterton, *J. Electrochem. Soc.* **1990**, *137*, 775–780.
[14] H. S. Kim, T. S. Arthur, G. D. Allred, J. Zajicek, J. G. Newman, A. E. Rodnyansky, A. G. Oliver, W. C. Boggess, J. Muldoon, *Nat. Commun.* **2011**, *2*, 2–6.

© 2019 Wiley-VCH Verlag GmbH & Co. KGaA, Weinheim

25666223, 2019, 9, Downloaded from https://chemistry-europe.onlinelibrary.wiley.com/doi/10.1002/batt.201900029 by University of Ulsan, Wiley Online Library on [11/11/2025]. See the Terms and Conditions (https://onlinelibrary.wiley.com/terms-and-conditions) on Wiley Online Library for rules of use; OA articles are governed by the applicable Creative Commons License

[15] Y. Guo, F. Zhang, J. Yang, F. Wang, Y. NuLi, S. Hirano, *Energy Environ. Sci.* **2012**, *5*, 9100–9106.
[16] T. Liu, Y. Shao, G. Li, M. Gu, J. Hu, S. Xu, Z. Nie, X. Chen, C. Wang, J. Liu, *J. Mater. Chem. A* **2014**, *2*, 3430–3438.
[17] T. Liu, J. T. Cox, D. Hu, X. Deng, J. Hu, M. Y. Hu, J. Xiao, Y. Shao, K. Tang, J. Liu, *Chem. Commun.* **2015**, *51*, 2312–2315.
[18] S. He, J. Luo, T. L. Liu, *J. Mater. Chem. A* **2017**, *5*, 12718–12722
[19] J. Luo, S. He, T. L. Liu, *ACS Energy Lett.* **2017**, *2*, 1197–1202.
[20] Y. Bi, J. Luo, B. Hu, S. He, K. Nielson, T. L. Liu, *ECS Trans.* **2017**, *80*, 343–348.
[21] R. Mohtadi, M. Matsui, T. S. Arthur, S.-J. Hwang, *Angew. Chem. Int. Ed.* **2012**, *51*, 9780–9783; *Angew. Chem.* **2012**, *124*, 9918–9921.
[22] Y. Shao, T. Liu, G. Li, M. Gu, Z. Nie, M. Engelhard, J. Xiao, D. Lv, C. Wang, J.-G. Zhang, J. Liu, *Sci. Rep.* **2013**, *3*, 3130.
[23] Z. Zhao-Karger, X. Zhao, O. Fuhr, M. Fichtner, *RSC Adv.* **2013**, *3*, 16330–16335.
[24] R. E. Doe, R. Han, J. Hwang, A. J. Gmitter, I. Shterenberg, H. D. Yoo, N. Pour, D. Aurbach, *Chem. Commun.* **2014**, *50*, 243–245.
[25] C. J. Barile, E. C. Barile, K. R. Zavadil, R. G. Nuzzo, A. A. Gewirth, *J. Phys. Chem. C* **2014**, *18*, 27623–27630.
[26] T. J. Carter, R. Mohtadi, T. S. Arthur, F. Mizuno, R. Zhang, S. Shirai, J. W. Kampf, *Angew. Chem. Int. Ed.* **2014**, *53*, 3173–3177; *Angew. Chem.* **2014**, *126*, 3237–3241.
[27] E. G. Nelson, S. I. Brody, J. W. Kampf, B. M. Bartlett, *J. Mater. Chem. A* **2014**, *2*, 18194–18198.
[28] C. J. Barile, R. G. Nuzzo, A. A. Gewirth, *J. Phys. Chem. C* **2015**, *119*, 13524–13534.
[29] C. Liao, N. Sa, B. Key, A. K. Burrell, L. Cheng, L. A. Curtiss, J. T. Vaughey, J.-J. Woo, L. Hu, B. Pan, Z. Zhang, *J. Mater. Chem. A* **2015**, *3*, 6082–6087.
[30] B. Pan, J. Zhang, J. Huang, J. T. Vaughey, L. Zhang, S.-D. Han, A. K. Burrell, Z. Zhang, C. Liao, *Chem. Commun.* **2015**, *51*, 6214–6217.
[31] Z. Zhao-Karger, X. Zhao, D. Wang, T. Diemant, R. J. Behm, M. Fichtner, *Adv. Energy Mater.* **2015**, *5*, 1401155–1401163.
[32] Y. Cheng, R. M. Stolley, K. S. Han, Y. Shao, B. W. Arey, N. M. Washton, K. T. Mueller, M. L. Helm, V. L. Sprenkle, J. Liu, G. Li, *Phys. Chem. Chem. Phys.* **2015**, *17*, 13307–13314.
[33] E. V. Brouillet, A. R. Kennedy, K. Koszinowski, R. McLellan, R. E. Mulvey, S. D. Robertson, *Dalton Trans.* **2016**, *45*, 5590–5597.
[34] J. H. Ha, B. Adams, J.-H. Cho, V. Duffort, J. H. Kim, K. Y. Chung, B. W. Cho, L. F. Nazar, S. H. Oh, *J. Mater. Chem. A* **2016**, *4*, 7160–7164.
[35] B. Pan, J. Huang, M. He, S. M. Brombosz, J. T. Vaughey, L. Zhang, A. K. Burrell, Z. Zhang, C. Liao, *ChemSusChem* **2016**, *9*, 595–599.
[36] N. Sa, B. Pan, A. Saha-Shah, A. A. Hubaud, J. T. Vaughey, L. A. Baker, C. Liao, A. K. Burrell, *ACS Appl. Mater. Interfaces* **2016**, *8*, 16002–16008.
[37] J. T. Herb, C. A. Nist-Lund, C. B. Arnold, *J. Mater. Chem. A* **2017**, *5*, 7801–7805.
[38] S.-J. Kang, S.-C. Lim, H. Kim, J. W. Heo, S. Hwang, M. Jang, D. Yang, S.-T. Hong, H. Lee, *Chem. Mater.* **2017**, *29*, 3174–3180.
[39] W. Li, S. Cheng, J. Wang, Y. Qiu, Z. Zheng, H. Lin, S. Nanda, Q. Ma, Y. Xu, F. Ye, M. Liu, L. Zhou, Y. Zhang, *Angew. Chem. Int. Ed.* **2016**, *55*, 6406–6410; *Angew. Chem.* **2016**, *128*, 6516–6520.
[40] T. Gao, S. Hou, F. Wang, Z. Ma, X. Li, K. Xu, C. Wang, *Angew. Chem. Int. Ed.* **2017**, *56*, 13526–13530; *Angew. Chem.* **2017**, *129*, 13711–13715.
[41] Z. Zhao-Karger, J. E. Mueller, X. Zhao, O. Fuhr, T. Jacob, M. Fichtner, *RSC Adv.* **2014**, *4*, 26924–26927.
[42] Z. Lu, A. Schechter, M. Moshkovich, D. Aurbach, *J. Electroanal. Chem.* **1999**, *466*, 203–217.
[43] O. Mizrahi, N. Amir, E. Pollak, O. Chusid, V. Marks, H. Gottlieb, L. Larush, E. Zinigrad, D. Aurbach, *J. Electrochem. Soc.* **2008**, *155*, A103–A109.
[44] N. Pour, Y. Gofer, D. T. Major, D. Aurbach, *J. Am. Chem. Soc.* **2011**, *133*, 6270–6278.
[45] J. Muldoon, C. B. Bucur, A. G. Oliver, J. Zajicek, G. D. Allred, W. C. Boggess, *Energy Environ. Sci.* **2013**, *6*, 482–487.
[46] D. Aurbach, I. Weissman, Y. Gofer, E. Levi, *Chem. Rec.* **2003**, *3*, 61–73.
[47] S. Sakamoto, T. Imamoto, K. Yamaguchi, *Org. Lett.* **2001**, *3*, 1793–1795.
[48] I. Shterenberg, M. Salama, H. D. Yoo, Y. Gofer, J.-B. Park, Y.-K. Sun, D. Aurbach, *J. Electrochem. Soc.* **2015**, *162*, A7118–A7128.
[49] O. Tutusaus, R. Mohtadi, T. S. Arthur, F. Mizuno, E. G. Nelson, Y. V. Sevryugina, *Angew. Chem. Int. Ed.* **2015**, *54*, 7900–7904; *Angew. Chem.* **2015**, *127*, 8011–8015.
[50] S. G. McArthur, L. Geng, J. Guo, V. Lavallo, *Inorg. Chem. Front.* **2015**, *2*, 1101–1104.
[51] S. G. McArthur, R. Jay, L. Geng, J. Guo, V. Lavallo, *Chem. Commun.* **2017**, *53*, 4453–4456.
[52] J. T. Herb, C. A. Nist-Lund, C. B. Arnold, *ACS Energy Lett.* **2016**, *1*, 1227–1232.
[53] Z. Zhang, Z. Cui, L. Qiao, J. Guan, H. Xu, X. Wang, P. Hu, H. Du, S. Li, X. Zhou, S. Dong, Z. Liu, G. Cui, L. Chen, *Adv. Energy Mater.* **2017**, *7*, 1602055.
[54] Z. Zhao-Karger, M. E. Gil Bardaji, O. Fuhr, M. Fichtner, *J. Mater. Chem. A* **2017**, *5*, 10815–10820.
[55] H. Xu, Z. Zhang, Z. Cui, A. Du, C. Lu, S. Dong, J. Ma, X. Zhou, G. Cui, *Electrochem. Commun.* **2017**, *83*, 72–76.
[56] J. Luo, Y. Bi, L. Zhang, X. Zhang, T. L. Liu, *Angew. Chem. Int. Ed.* **2019**, *58*, 6967–6971.
[57] P. Canepa, S. Jayaraman, L. Cheng, N. N. Rajput, W. D. Richards, G. S. Gautam, L. A. Curtiss, K. A. Persson, G. Ceder, *Energy Environ. Sci.* **2015**, *8*, 3718–3730.
[58] J. G. Connell, B. Genorio, P. P. Lopes, D. Strmcnik, V. R. Stamenkovic, N. M. Markovic, *Chem. Mater.* **2016**, *28*, 8268–8277.
[59] D. Aurbach, A. Schechter, M. Moshkovich, Y. Cohen *J. Electrochem. Soc.* **2001**, *148*, A1004–A1014.
[60] A. Benmayza, M. Ramanathan, T. S. Arthur, M. Matsui, F. Mizuno, J. Guo, P.-A. Glans, J. Prakash, *J. Phys. Chem. C* **2013**, *117*, 26881–26888.
[61] K. A. See, K. W. Chapman, L. Zhu, K. M. Wiaderek, O. J. Borkiewicz, C. J. Barile, P. J. Chupas, A. A. Gewirth, *J. Am. Chem. Soc.* **2016**, *138*, 328–337.
[62] L. F. Wan, D. Prendergast, *J. Am. Chem. Soc.* **2014**, *136*, 14456–14464.
[63] Y. Zhao, D. G. Truhlar, *Acc. Chem. Res.* **2008**, *41*, 157–167.
[64] R. Krishnan, J. S. Binkley, R. Seeger, J. A. Pople, *J. Chem. Phys.* **1980**, *72*, 650–654.
[65] A. D. Mclean, G. S. Chandler, *J. Chem. Phys.* **1980**, *72*, 5639–5648.
[66] Y. Zhao, D. G. Truhlar, *Theor. Chem. Acc.* **2008**, *120*, 215–241.
[67] Y. Zhao, D. G. Truhlar, *Chem. Phys. Lett.* **2011**, *502*, 1–13.
[68] N. Mardirossian, M. Head-Gordon, *J. Chem. Theory Comput.* **2016**, *12*, 4303–4325.
[69] H. Kruse, L. Goerigk, S. Grimme, *J. Org. Chem.* **2012**, *77*, 10824–10834.
[70] A. V. Marenich, C. J. Cramer, D. G. Truhlar, *J. Phys. Chem. B* **2009**, *113*, 6378–6396.
[71] A. W. Addison, T. N. Rao, J. Reedijk, J. van Rijn, G. C. Verschoor, *J. Chem. Soc. Dalton Trans.* **1984**, 1349–1356.
[72] J. Tammiku-Taul, P. Burk, A. Tuulmets, *J. Phys. Chem. A* **2004**, *108*, 133–139.

Manuscript received: February 20, 2019
Revised manuscript received: June 5, 2019
Accepted manuscript online: June 5, 2019
Version of record online: July 4, 2019

© 2019 Wiley-VCH Verlag GmbH & Co. KGaA, Weinheim

25666223, 2019, 9, Downloaded from https://chemistry-europe.onlinelibrary.wiley.com/doi/10.1002/batt.201900029 by University of Ulsan, Wiley Online Library on [11/11/2025]. See the Terms and Conditions (https://onlinelibrary.wiley.com/terms-and-conditions) on Wiley Online Library for rules of use; OA articles are governed by the applicable Creative Commons License